Available online at www.sciencedirect.com
ScienceDirect
Bioorganic & Medicinal Chemistry 15 (2007) 6407–6417
Bioorganic & Medicinal Chemistry

Construction of a three-dimensional pharmacophore for Bcl-2 inhibitors by flexible docking and the multiple copy simultaneous search method

Can-Hui Zheng,[a] You-Jun Zhou,[a,*] Ju Zhu,[a] Hai-Tao Ji,[b] Jun Chen,[a] Yao-Wu Li,[a] Chun-Quan Sheng,[a] Jia-Guo Lu,[a] Jun-Hang Jiang,[a] Hui Tang[a] and Yun-Long Song[a]

[a]*Department of Medicinal Chemistry, School of Pharmacy, Second Military Medical University, 325 Guohe Road, Shanghai 200433, China*
[b]*Department of Chemistry, Biochemistry, Molecular Biology, and Cell Biology, and Center for Drug Discovery and Chemical Biology, Northwestern University, Evanston, IL 60208-3113, USA*

Received 13 April 2007; revised 23 June 2007; accepted 27 June 2007
Available online 4 July 2007

Abstract—B-Cell lymphoma-2 (Bcl-2) protein is a new promising target for anticancer drugs. A number of anticancer Bcl-2 inhibitors with diverse chemical structures have been discovered in recent years. In this paper, the flexible docking was performed to determine the binding modes of the representative inhibitors from different structural types. Subsequently, the binding modes of inhibitor were used to construct a primary three- dimensional (3D) pharmacophore model. It proved that this model can effectively disrupt the binding of the BH3 domain of proapoptotic Bcl-2 family members to Bcl-2, and match the structural requirement of a new type of Bcl-2 inhibitors. However, these distances between pharmacophoric points are not optimal due to the fact that not all of individual functional groups are located in the ideal position when inhibitors bind to its receptor. In this paper, we proposed a new idea to improve the quality of the pharmacophore model: the multiple copy simultaneous search (MCSS) method was performed to determine the energetically favorable distribution of functional groups with similar features to these pharmacophoric points in the active site of Bcl-2 first. Then their most energetically favorable minima in the positions near the pharmacophoric points were used to optimize the distances between pharmacophoric points. By examining the binding modes of several inhibitors from the same structural type, it was found that the more potent the inhibitor was, the closer it was to the optimized distances between pharmacophoric points. The optimized 3D pharmacophore model obtained in this paper may provide a good starting point for further rational design of Bcl-2 inhibitors.

1. Introduction

The Bcl-2 family of proteins plays important roles in the regulation of cellular apoptosis and is divided into two classes: antiapoptosis members (including Bcl-2) and proapoptosis members.[1,2] It has been revealed that antiapoptotic members inhibit apoptosis by antagonizing the actions of proapoptotic members.[3] And their activity is mediated through the association of a large hydrophobic pocket on the antiapoptotic members with the BH3 domain of the proapoptotic members.[4–6]

The overexpression of Bcl-2, which is found in a wide variety of human cancers, is associated with tumor progression and resistance to anti-cancer therapy.[7,8] Therefore, Bcl-2 is an attractive target for the development of anticancer agents.[9,10] In recent years, a number of small molecule compounds with diverse chemical structures have been identified as anticancer agents,[11–13] which can bind in the hydrophobic pocket on Bcl-2 and block its function.[14–20] And the 3D NMR structure of the Bcl-2: a small molecule inhibitor complex (PDB code 1YSW) reported recently[20] extended our understanding of the binding modes between inhibitors and the active site of Bcl-2.

The enormous molecular diversity among the Bcl-2 inhibitors presents a significant challenge to determining the essential structural features for activity. Therefore, no detailed 3D pharmacophore model for Bcl-2

Keywords: Bcl-2 inhibitor; Three-dimensional pharmacophore; Pharmacophoric points; Flexible docking; Multiple copy simultaneous search (MCSS).
* Corresponding author. Tel.: +86 021 25070383; e-mail: zhouyoujun2006@yahoo.com.cn

0968-0896/$ - see front matter © 2007 Elsevier Ltd. All rights reserved.
doi:10.1016/j.bmc.2007.06.052

inhibitors has been determined until now, though it can provide useful insights for rational inhibitor design.[21] In this paper, we performed flexible docking to construct binding modes for the representative inhibitors from different structural types. Subsequently, examination of the binding modes of inhibitor revealed a primary 3D pharmacophore model, in which the distances between pharmacophoric points were calculated based on the bioactive conformation of the representative inhibitors. To assess the reliability of this pharmacophore model, we examined whether or not it can effectively disrupt Bcl-2 binding to the BH3 domain of proapoptotic Bcl-2 family members, and match the structural requirement of a new type of Bcl-2 inhibitors.

However, it was found that not all of individual functional groups were located in the ideal position when inhibitors were binding to its receptor, though the inhibitors possessed high affinity.[20,22,23] Figure 1a shows the comparison between the NMR structures of an inhibitor (PDB code 1YSI) and the functional groups composing it (PDB code 1YSG) in complex with the Bcl-x_L protein.[20,23] Therefore, the distances between pharmacophoric points in the primary 3D pharmacophore model are not optimal.

The MCSS method can effectively determine energetically favorable positions and orientations of functional groups for a target macromolecule with known 3D structures based on a combination of Monte Carlo and energy minimization techniques.[24–26] It has been reported that the binding conformation of MVT-101 (an inhibitor of HIV-1 aspartic proteinase) constructed by the MCSS resulting minima corresponds well with that in the cocrystal structure.[24] In this paper, we proposed a new idea to improve the quality of the pharmacophore model of Bcl-2 inhibitors. The MCSS method was used to determine the optimal positions and orientations of functional groups with similar features to the pharmacophoric points in the active site of Bcl-2 first. Then the most energetically favorable minima in the positions near the pharmacophoric points were used to optimize the distances between pharmacophoric points. To validate the results, we examined whether the more potent inhibitor was closer to the optimized distances between pharmacophoric points than other inhibitors from the same structural type. The optimized 3D pharmacophore model obtained in this paper may provide a good starting point for further rational design of Bcl-2 inhibitors.

2. Results and discussion

The active site of Bcl-2 was found to be a narrow and long groove filled with 722 grid points (722 Å^3) on the protein surface, using the Binding Site Analysis program. As shown in Figure 1b, the bottom of it is bound by α5, and on the side, it is bound by α2, α3, α4, and α8. The active site comprises five main areas from the standpoint of drug design. The P1, P2 are two big and deep pockets in the active site. The P3, P4 are two small pockets at two ends of the active site. And the L1 is a narrow and shallow channel linking P1 and P2.

2.1. The binding modes of the representative inhibitors

Figure 2 shows the representative Bcl-2 inhibitors selected. [1–10] They are the most potent inhibitors from different structural types,[14–20] in addition to **1**, the inhibitor from the NMR structure (PDB code: 1YSW).

Figure 3 shows the binding modes of **1**–**10** in the Bcl-2 active site. The binding modes of **1** and **2**[27] are reasonable because they were determined based on the 3D NMR structure 1YSW directly and indirectly, respectively. To evaluate the binding modes of the other inhibitors, we examined whether they can elucidate the known structure-activity relationship (SAR). The binding mode of **6** which was obtained in our previous studies[28] explains the good Bcl-2 selectivity versus Bcl-x_L. The binding modes of **3**, **5**, **7**, and **8** can explain the much lower affinities of their corresponding derivatives **13**, **19**, **12**, and **11**, respectively.[15,16,18] And the binding

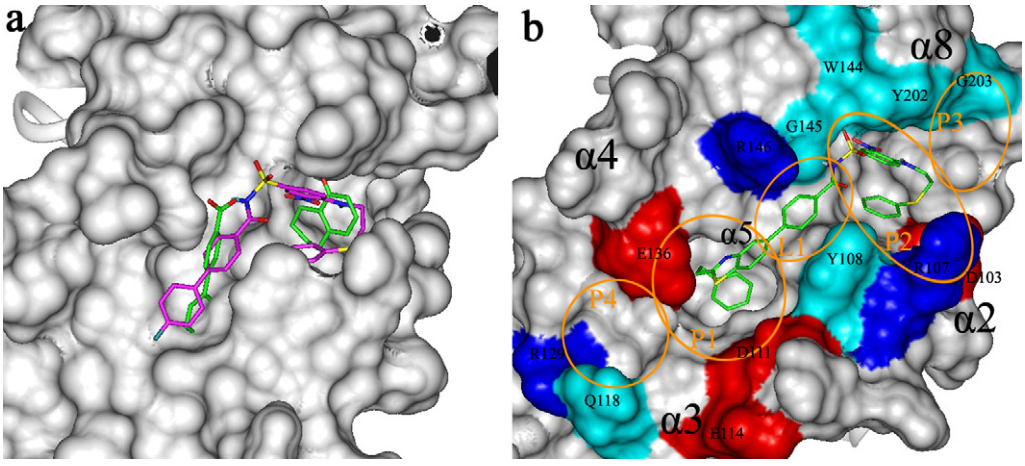

Figure 1. (a) Comparison between the NMR structures of an inhibitor (1YSI) and the functional groups composing it (1YSG) in complex with the Bcl-x_L protein. They are shown in stick with the carbon atoms of the inhibitor colored purple and the carbon atoms of the functional groups green. (b) Schematic representation of the active site of Bcl-2. Inhibitor **1** binding to it is shown in stick.

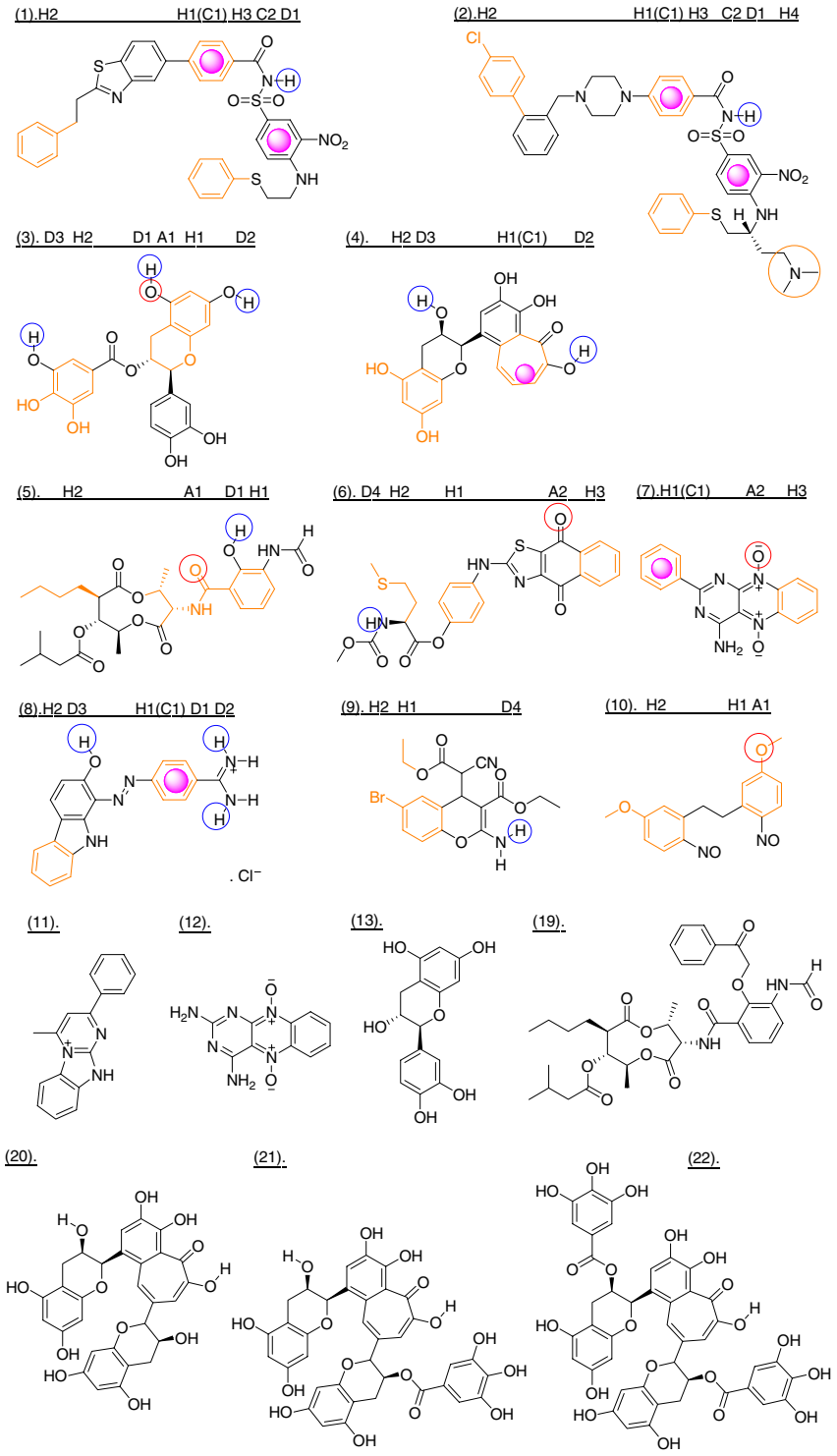

Figure 2. The structures of the representative inhibitors **1**–**10** and some derivatives. The yellow lines denote the functional groups that comprise pharmacophoric points H1, H2, and H3, respectively. The red, blue, and yellow circles represent hydrogen bond acceptors, hydrogen bond donors, and H4, respectively. The purple spheres represent large conjugated systems.

mode of **4** can explain why its derivatives **20**, **21** can bind to the active site of Bcl-2, while **22** cannot.[18]

Each binding mode of the representative inhibitors was evaluated using the score functions[43,44] in the LUDI module within InsightII (the results are shown in Table 1). They are the knowledge-based free energy calculation functions which are theoretically correlated with the affinities of inhibitors. However, as shown in Table 1, the affinities of the representative inhibitors were from different literature sources.[14,15,18,29,39] The affinities of some inhibitors are presented by their IC50 values, and the others are the K_i values. An equation was particularly developed to convert IC50 values into K_i values

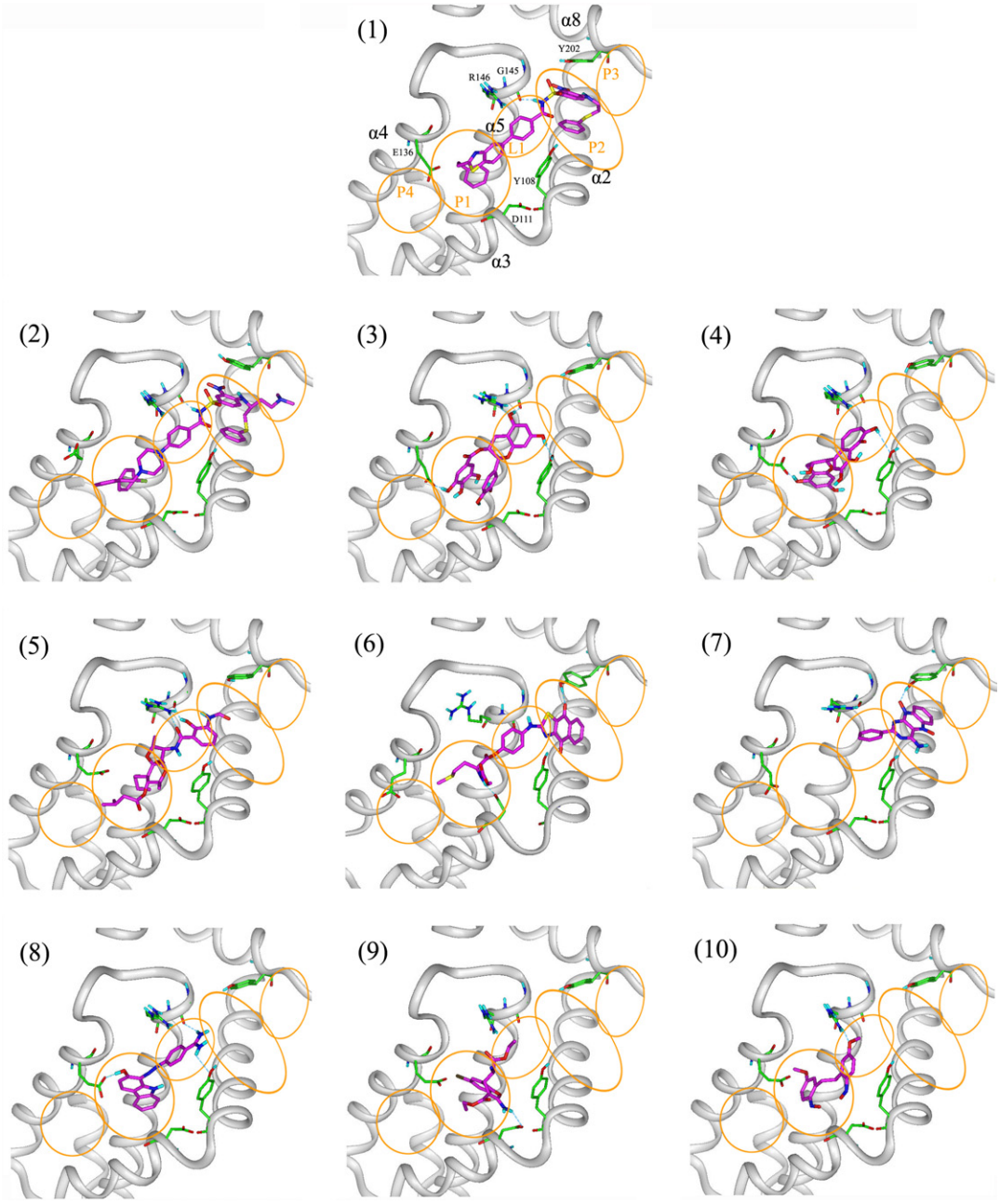

Figure 3. Binding modes of the representative inhibitors **1**–**10**. The backbones of Bcl-2 are rendered as gray ribbons. Side chains of important residues in the Bcl-2 active site and **1**–**10** are shown in stick with the carbon atoms of Bcl-2 colored green and the carbon atoms of inhibitors purple. Cyan dashed lines indicate intermolecular hydrogen bonds. The compound number is at the top left corner of each panel.

for fluorescence polarization (FP) assays.[45] But we cannot convert the IC50 values into K_i values of the representative inhibitors in this paper due to the lack of the K_d values of the substrate in their FP assays. Furthermore, the IC50 values of some inhibitors still cannot be used to compare with each other directly because different experimental conditions were used in the FP assays. Therefore, we only compared the affinities of the inhibitors determined in the identical condition with their binding scores. The trend for LUDI scores 2 is in good qualitative agreement with the affinities of the inhibitors determined in the identical condition, though there is no high correlation between them due to their different structural types. However, as shown in Table 6, the LUDI scores 2 of a new type of inhibitors **14**–**17** from the same structural type (the structures shown in Fig. 5, and the binding modes of them discussed in detail in page 8) correlated well with their K_i values[39] ($R^2 = 0.95$), implying that the established binding modes of inhibitors are reasonable.

2.2. Construction of the 3D pharmacophore model

Table 1 shows twelve types of interaction of these ten inhibitors with Bcl-2. On the basis of these twelve types of inhibitor-Bcl-2 interaction, 12 possible corresponding

Table 1. Interactions with Bcl-2 and corresponding pharmacophoric points (last column) of the representative inhibitors **1**–**10**

	1	**2**	**3**	**4**	**5**	**6**	**7**	**8**	**9**	**10**	Points
Number of representative low energy conformations for docking	1	1	2	2	1	1	1	1	2	1	
Interactions with Bcl-2[a]											
Van der Walls interaction with L1	√	√	√	√	√	√	√	√	√	√	H1
Van der Walls interaction with P1	√	√	√	√	√	√		√	√	√	H2
Van der Walls interaction with P2	√	√				√	√				H3
Hydrogen bond (with the backbone carbonyl of G145)	√	√	√		√			√			D1
Cation-π interaction (with R146)	√	√		√			√	√			C1
Hydrogen bond (with the hydroxyl of Y108)			√	√				√			D2
Hydrogen bond (with R146)			√		√					√	A1
Hydrogen bond (with E136)			√	√				√			D3
Hydrogen bond (with D111)						√			√		D4
Hydrogen bond (with the hydroxyl of Y202)						√	√				A2
π–π interaction (with Y202)	√	√									C2
Van der Walls interaction with P3		√									H4
Scores 1[b]	830	898	689	691	377	833	586	619	557	469	
Scores 2[b]	473	640	393	346	386	388	348	345	311	338	
Affinity											
IC50 from Ref. 15 (μM)							1.6 ± 0.1	5.8 ± 2.2		10.4 ± 0.3	
IC50 from Ref. 14 (μM)									9		
IC50 from Ref. 29 (μM)		0.12			2.95	6.43					
K_i from Ref. 18 (μM)			0.230	0.286							

[a] The inhibitors interact with the side chain of residues depicted in the table, except those indicated in particular which interact with the backbone of residues.

[b] The scores were computed by the LUDI module of InsightII. The difference between the score 1 and score 2 is that an additional term evaluating the contribution of binding of aromatic-aromatic interaction is added to LUDI score 1.[43,44]

pharmacophoric points were selected. As shown in Table 1 and Figure 2, it consists of four hydrophobic centers (H1, H2, H3, and H4), four hydrogen bond donors (D1, D2, D3, and D4), two hydrogen bond acceptors (A1 and A2), and two large conjugated systems (C1 and C2). Nevertheless, their roles in inhibitor binding are different from each other. Figure 4a depicts the pharmacophoric points mapped onto the superimposition of **1**–**10** in the active site of Bcl-2. Points H2–H1–H3 were found to serve as a linear molecular scaffold that satisfy the overall geometric and steric requirements for inhibitor binding. The Van der Walls interactions around these pharmacophoric points play major roles in binding to Bcl-2. Based on the structures of **1**–**10**, we propose that a effective Bcl-2 inhibitor should be a linear molecule including point H1 and at least one of H2 and H3, and the inhibitors including H1, H2 and H3 simultaneously would be highly potent. This conclusion is consistent with that suggested[18] for Bcl-x_L on the basis of the studies of tea polyphenols, such as **3** and **4**. They suggested that compounds capable of occupying all three of the subpockets of the active site, which correspond to the hydrophobic centers H1, H2, and H3 in this paper, exhibit the strongest binding. However, the detailed pharmacophoric points and distances between them were not discussed in the original paper.[18]

In addition, points D1, C1, D2, A1, and D3 occur in the binding modes of the representative inhibitors frequently. They can form electrostatic interactions with Bcl-2 and improve affinity and specificity. However, points D4, A2, C2, and H4, which are able to enhance the affinity of inhibitors further, occur in the binding modes of the representative inhibitors less frequently. Figure 4b highlights the interactions between the pharmacophoric points and the active site of Bcl-2. Figure 4c shows the calculated distances between pharmacophoric points based on the bioactive conformations of the representative inhibitors, which construct the primiry 3D pharmacophore model.

Because the small molecule inhibitors mimic the BH3 domains of the proapoptotic members to bind into the active site of Bcl-2, we compared the pharmacophore model with the key binding points of the BH3 domains of the proapoptotic members to assess the reliability of the model. We examined the interactions between substrate BH3 peptides and the proteins (see Table 2) on the basis of the 3D structure of the complexes.[4,6,30] The complex structures of Bcl-x_L were included in discussion because of the high homology and similar property between Bcl-2 and Bcl-x_L. Though mouse-derived it is, structure 1PQ1 was also included because mouse-derived and human-derived Bcl-x_L only differ in two residues which are far from the active site. While no complex structure of Bcl-2 was determined at present, the homologous 3D model of Bcl-2 in complex with the BH3 peptide of Bak constructed in our previous studies[31] provides an approximate template.

As shown in Table 2, it was found that the formation of all of the complex was mainly attributed to several

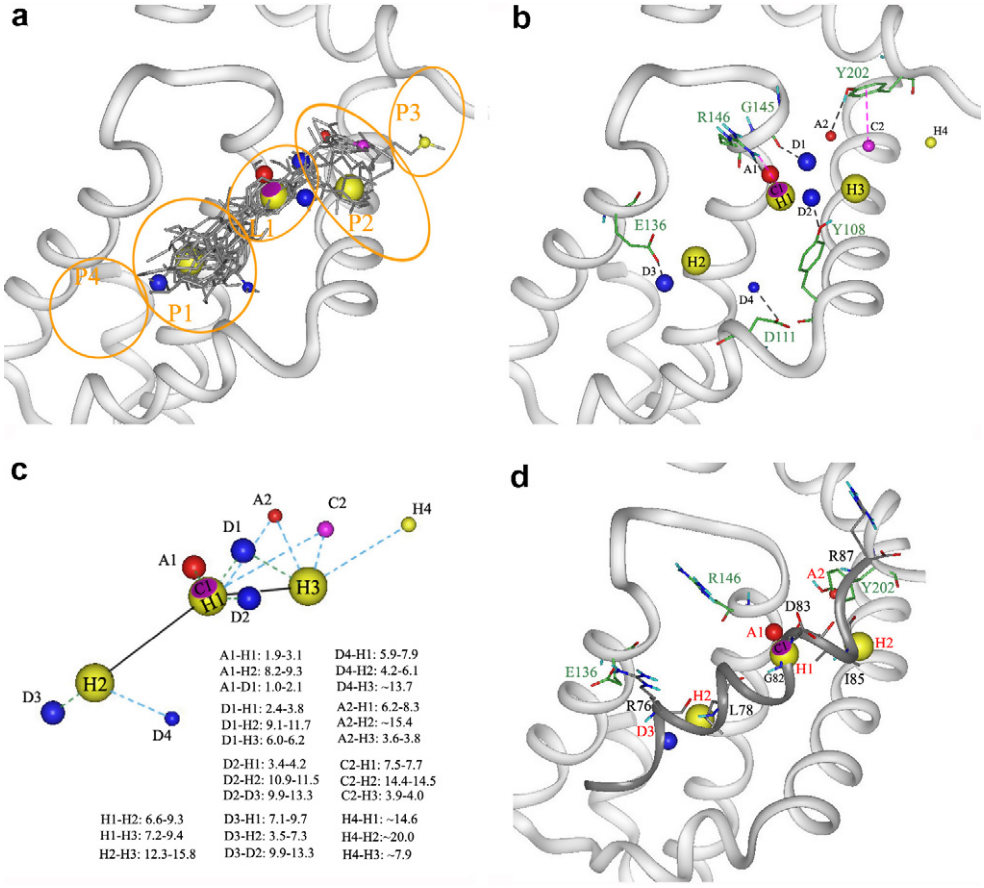

Figure 4. (a) Pharmacophoric points (shown in spheres colored as Fig. 2) mapped onto the superimposition of **1**–**10** (shown in dark gray sticks) in the Bcl-2 active site (backbones shown in gray ribbons). (b) Interactions between the pharmacophoric points and the Bcl-2 active site (backbones shown in gray ribbons and side chains shown in sticks with carbon atoms colored in green). (c) Primary 3D pharmacophore model of inhibitors of Bcl-2. The distances between pharmacophoric points (Å) are shown. (d) Pharmacophoric points superimposed onto the homologous 3D model of Bcl-2 in complex with the BH3 peptide of Bak (backbones shown in dark gray ribbons and side chains shown in sticks with carbon atoms colored in dark gray).

interactions, including the Van der Walls interactions with P1, P2, and L1 areas in the active site, and the electrostatic interactions or hydrogen bonds with R146 and E136 of Bcl-2 (R139 and E129 of Bcl-x_L). These interactions play important roles in the binding between substrate BH3 peptides and the proteins. This is supported by a number of mutations in the active site of Bcl-2[32,33] and Bcl-x_L,[6,34–36] and alanine mutations in BH3 domains of the proapoptotic members,[6,37] which have been shown to inhibit their function. These key binding points of the BH3 peptides correspond to the important pharmacophoric points H2, H3, H1, A1, and D3 in our model, respectively.

As shown in Figure 4d, we superimposed the pharmacophore model onto the homologous 3D model of Bcl-2 in complex with the BH3 peptide of Bak. The pharmacophoric point H1 superimposes with the Bak backbone atoms which bind to the L1 area of the Bcl-2 active site, and points H2, H3 can disrupt Bcl-2 binding to two critical hydrophobic residues of Bak (L78 and I85), respectively. Additionally, points A1, D3, and A2 can competitively inhibit important electrostatic interactions between the BH3 peptide of Bak and Bcl-2. The effective disruption of the binding between the BH3 domain and Bcl-2 confirms the reasonability of the pharmacophore model.

On the basis of the modeling of complex structures and molecular dynamics computation, the minimum requirements for a hexadecapeptide to interact with Bcl-2 were established.[38] Besides three hydrophobic residues in positions 7, 10, and 14, it requires the existence of a charged residue in positions 12 and 13. Affinity can be increased by an additional positively charged residue in positions 5 and 8, and a negatively charged residue in position 15. Though the detailed spatial relationship of these positions was not discussed, it was proposed that these positions can be used to search small molecule inhibitors. This proposition was confirmed in this paper. The important positions of hexadecapeptides are corresponding, respectively, to the important pharmacophoric points H2, H1, H3, A1, and D3 in our pharmacophore model for small molecule inhibitors.

In addition, after we completed the construction of the pharmacophore model, a new type of Bcl-2 inhibitors

Table 2. The key interactions between substrate BH3 peptides and Bcl-2, Bcl-x_L and corresponding pharmacophoric points (last column)

Interactions with Bcl-2[a]	Bak BH3	Interactions with Bcl-x_L[a]	Bak BH3 (1BXL)	Bad BH3 (1G5J)	Bim BH3 (1PQ1)	Points
Van der Walls interaction with L1	I81	Van der Walls interaction with L1	I81	M154	I97	H1
Van der Walls interaction with P1	V74, L78	Van der Walls interaction with P1	V74, L78	Y147, L151	A91, L94	H2
Van der Walls interaction with P2	I85	Van der Walls interaction with P2	I85	F158, Val159	F101	H3
Hydrogen bond (with the backbone carbonyl of G145)		Hydrogen bond (with the backbone carbonyl of G138)			N102	D1
Cation-π interaction (with R146)		Cation-π interaction (with R139)				C1
Hydrogen bond (with the hydroxyl of Y108)		Hydrogen bond (with the hydroxyl of Y101)				D2
Electrostatic interaction or hydrogen bond (with R146)	D83	Electrostatic interaction or Hydrogen bond (with R139)	D83	D156	D99	A1
Electrostatic interaction or hydrogen bond (with E136)	R76	Electrostatic interaction or hydrogen bond (with E129)	R76	R149	Q92, R95	D3
Hydrogen bond (with D111)		Hydrogen bond (with D104)				D4
Hydrogen bond (with the hydroxyl of Y202)	R87	Hydrogen bond (with the hydroxyl of Y195)	I85, R87		N102	A2
π–π interaction (with Y202)		π–π interaction (with Y195)				C2
Van der Walls interaction with P3		Van der Walls interaction with P3		F162	Y105	H4
Van der Walls interaction with P4		Van der Walls interaction with P4		L141, A143, A144,	I90	
		Hydrogen bond (with E96)			Y105	
		Hydrogen bond (with Q125)			R85	
		Hydrogen bond (with N136)			D99	

[a] The inhibitors interact with the side chain of residues depicted in the table, except those indicated in particular which interact with the backbone of residues.

(**14**–**18**) was reported.[39] They were used to validate the pharmacophore model we constructed. The binding modes of **14**–**17** were determined by flexible docking (see Figure 6d–g). The binding modes are reasonable because they can elucidate that the binding affinity of **17** is higher than that of derivative **18** (see Figure 5), and the calculated Ludi scores 2 of the inhibitors correlate well with their K_i values (see Table 6). As shown in Figures 5 and 6d, the inhibitors consist of the three crucial pharmacophoric points P1, P2, P3, and A1, which explains the high affinity of **17** including all of these points. And the distances between pharmacophoric points mostly conform to the 3D pharmacophore model we constructed. That the 3D pharmacophore model can match the structural requirement of the new inhibitors, which are structurally distinct from the inhibitors used in the construction of the model, confirms the reliability of the model further. It suggested that the 3D pharmacophore model may be not only for the representative inhibitors in our paper, but also for all of the Bcl-2 inhibitors. In addition, this type of inhibitors still includes a hydrogen bond donor in the positions near the pharmacophoric point A2. It was found that either a hydrogen bond acceptor (A2) or a hydrogen bond donor (named D5) can be located in this position, due to the interaction with either the hydrogen or oxygen atom of the hydroxyl in Y202 side chain.

2.3. Optimized 3D pharmacophore model

The distances between pharmacophoric points in the primary 3D pharmacophore model are not optimal due to the fact that not all of individual functional groups are located in the ideal position when inhibitors bind to its receptor. To explore the optimized 3D pharmacophore model, the MCSS method was performed to calculate the energetically favorable positions and orientations of functional groups with similar features to these pharmacophoric points in the active site of Bcl-2 first. Benzene and propane groups were chosen to approximate the interactions around hydrophobic centers. Benzene groups can also approximate the interactions of large conjugated systems. And *N*-methylacetamide, methanol, and dimethyl ether groups were chosen to approximate the interactions of hydrogen bond donors and acceptors. The results for these functional groups used for the MCSS calculations are summarized in Table 3. Since the functional groups are competing with solvent for binding to the protein, only minima whose interaction energy was less than one-half of the solvation enthalpy (reflecting the free energy of solvation) were considered in the next step of analysis.[24,26]

Then the most energetically favorable minima of each functional group in the positions near the pharmacophoric points, except the minima forming more than one interaction with the protein simultaneously, were used to optimize the distances between pharmacophoric points. The selected minima are shown in bold in Tables 4 and 5, and are denoted by spheres or circles in Figures 6a and b. The optimized distances between pharmacophoric points calculated are described in Figure 6c,

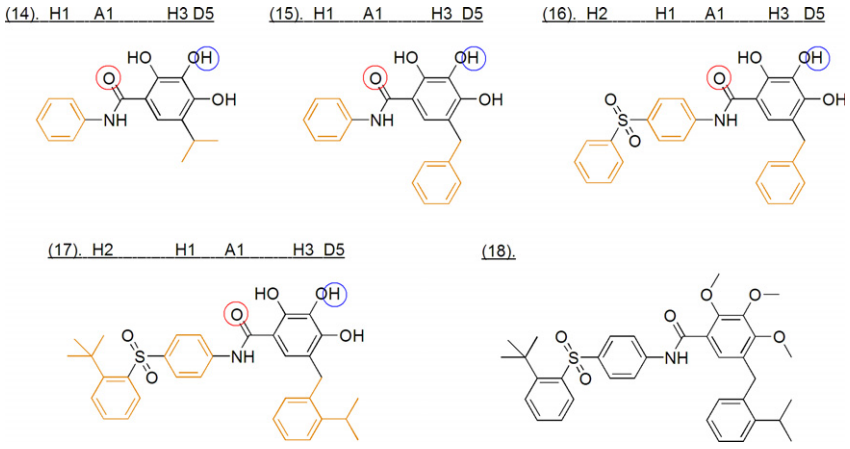

Figure 5. The structures of the inhibitors **14**–**18**. The pharmacophoric points are denoted as Figure 2.

which construct an optimized 3D pharmacophore model.

On the basis of the binding modes of inhibitors **14**–**17** from the same structural type, their distances between pharmacophoric points were calculated. It was found that the more potent inhibitor was closer to the optimized distances between pharmacophoric points than other inhibitors (see Table 6). This confirms the reasonability of our new idea to improve the quality of the pharmacophore model to a certain extent. It also implies that modifying this type of inhibitors to make them closer to the optimized distances between the pharmacophoric points can enhance their affinity.

Additionally, in the analysis of MCSS results, the hydrophobic groups were found to form clusters in hydrophobic areas P1 and P2 (near pharmacophoric points H2 and H3, respectively), due to the large volume of these areas. And some polar groups were found to form two clusters near point D3, because they can interact with residue E136 from two different directions, respectively. Since the energies of the most energetically favorable minima in each cluster are comparable, all of the minima are worth being considered in the inhibitor design.

3. Conclusions

In this paper, the binding modes of the representative Bcl-2 inhibitors from different structural types were determined by flexible docking. Subsequently, a primary 3D pharmacophore model was constructed based on the binding modes of inhibitor. This model proved to effectively disrupt the binding of the BH3 domain of proapoptotic Bcl-2 family members to Bcl-2, and match the structural requirement of a new type of Bcl-2 inhibitors. Then the energetically favorable positions and orientations of functional groups with similar features to these pharmacophoric points in the active site of Bcl-2 were determined by the MCSS method. And the distances between pharmacophoric points were optimized by the most energetically favorable minima in the positions near the pharmacophoric points. By examining the binding modes of several inhibitors from the same structural type, it was found that the more potent the inhibitor was, the closer the inhibitor was to the optimized distances between pharmacophoric points. The optimized 3D pharmacophore model obtained in this paper may provide a good starting point for further rational design of Bcl-2 inhibitors. The present paper additionally provides a new idea to determine a good 3D pharmacophore model, and further improvement of it is now underway.

4. Materials and methods

The 3D structures 1YSW, 1YSI, 1YSG, 1BXL, 1G5J, and 1PQ1 were obtained from RCSB Protein Data Bank. All calculations were performed on an Origin 300 Server with commercially available SYBYL6.9[40] and InsightII 2000[41] software packages.

4.1. Simple energy minimization of 3D NMR structure

The structures from RCSB Protein Data Bank were subjected to simple energy minimization to eliminate some distortion by MAXIMIN2 module within SYBYL using the following parameters: Tripos force filed, Kollman-all charges for atoms of the protein, Gasteiger-Hückel charges for atoms of the inhibitor, distance-dependent dielectric constant, and steepest descent minimization 100 steps, then conjugate gradient energy minimization until the root-mean-square (rms) gradient energy was lower than 0.5 kcal/mol Å. The restriction on the structure was relaxed gradually when energy minimization was performed.

4.2. Active site analysis

The size and spatial orientation of the active site were identified by grid analysis implemented in the Binding Site Analysis module within InsightII. The grid size for searching the proteins was set to 1 Å × 1 Å × 1 Å. All of the solvent accessible surfaces in the protein were filled with grid points and only those having at least 50 grid points were accepted as potential ligand binding sites.

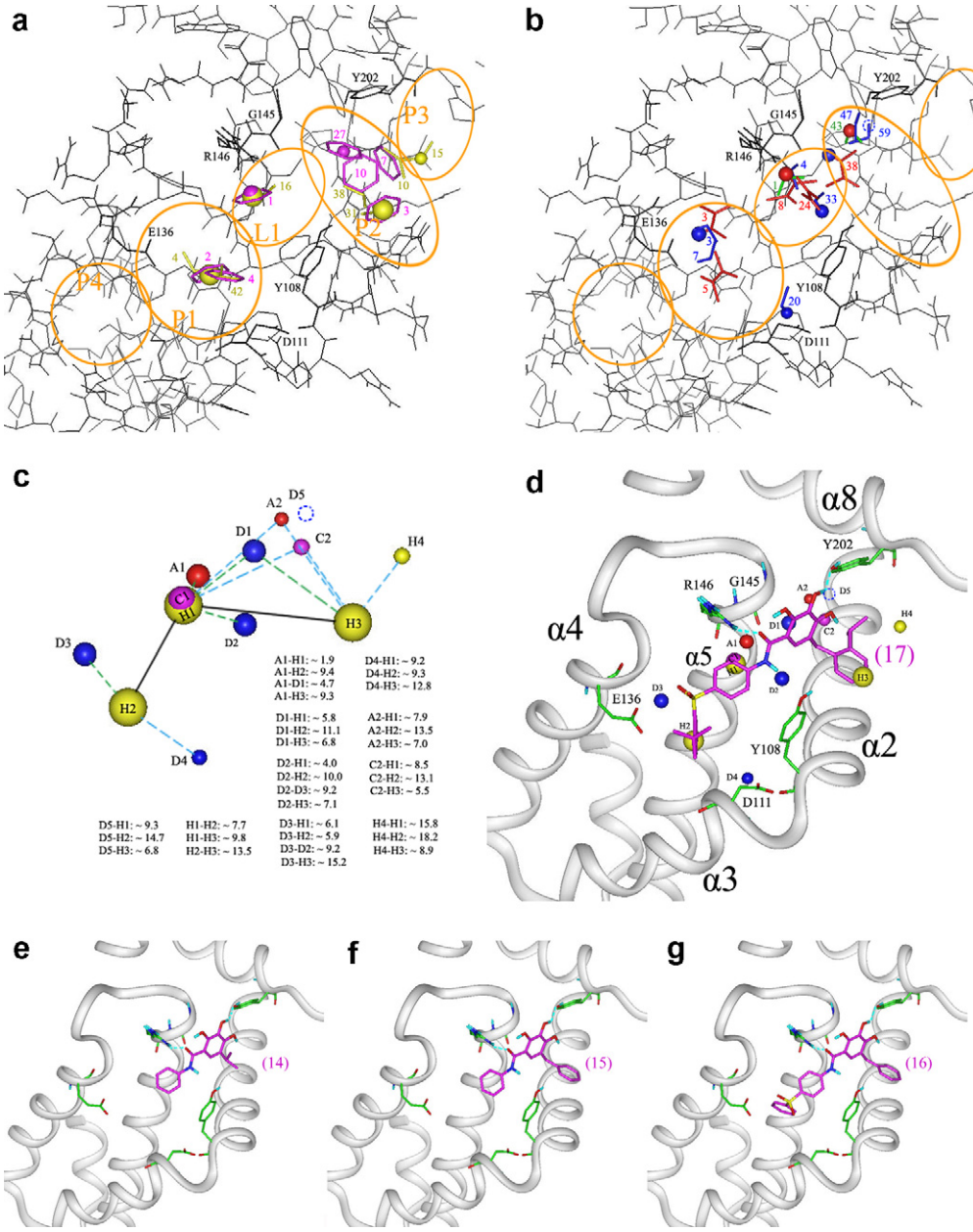

Figure 6. (a) Most energetically favorable minima of each cluster for hydrophobic functional groups (benzene shown in purple sticks and propane shown in yellow sticks) in the positions near the pharmacophoric points (protein shown in black sticks). The selected minima are denoted by spheres. (b) Most energetically favorable minima of each cluster for polar functional groups (*N*-methylacetamide shown in red sticks, methanol shown in blue sticks, and dimethyl ether shown in green) in the positions near the pharmacophoric points. (c) Optimized 3D pharmacophore model (D5 shown in blue dashed circle). The distances between pharmacophoric points (Å) are shown. (d) Pharmacophoric points mapped onto **17** binding to the active site of Bcl-2. (e–g) Binding modes of the inhibitors **14**–**16**. The compound number is bracketed in the figure.

Table 3. Results for functional groups used for the MCSS calculations

Functional groups*	ΔH/2 (kcal/mol)	Initial no. of copies	Minima with interaction energy <0	Range of interaction energy (kcal/mol)		Minima with interaction energy <ΔH/2
				From	To	
Benzene	−3.5	2000	30	−14.1	−3.45	29
Propane	−2.4	2000	75	−6.5	−2.84	75
N-Methylacetamide	−9.6	2000	58	−40.2	−3.20	46
Methanol	−5.1	2000	71	−27.7	−2.94	68
Dimethyl ether		2000	43	−17.5	−3.4	

Table 4. Most energetically favorable minima of each cluster for hydrophobic functional groups in the positions near the pharmacophoric points

Points	H1(C1)	H2	H3	H4	C2
Benzene	**1 (−14.1)**[a]	**2 (−13.8)** 4 (−12.4)	**3 (−12.5)** 7 (−11.8) 10 (−9.9)		**27 (−4.6)**
Propane	16 (−5.5)	4 (−6.0) 42 (−4.5)	10 (−5.8) 31 (−5.0) 38 (−4.7)	**15 (−5.5)**	

The serial number and bracketed interaction energy (unit: kcal/mol) of minima are shown. The selected minima are shown in bold.
[a] This group approximates both the interactions of H1 and C1.

4.3. Flexible docking of inhibitors into the active site

Small molecule inhibitors were built by SYBYL. After energy minimization and simulated annealing were performed, the representative low energy conformations of each inhibitor were selected for molecular docking (the numbers of those conformations for each inhibitor are listed in the first row of Table 1).

The flexible ligand docking procedure in the Affinity module within InsightII was used. The 1YSW structure after energy minimization was used as the protein template. All the atoms of inhibitors and the side chain of residues within a defined radius (8 Å) of inhibitors were allowed to move freely. The backbone atoms of the residues, which were found involving obvious induced fit when substrate binding in our previous analysis,[27] were allowed to move with restriction. The solvation grid supplied with the affinity program was used.[42] If the resulting inhibitor/enzyme system was within a predefined energy tolerance of the previous structure, the system was subjected to minimization. The resulting structure was accepted on the basis of energy check, which used the Metropolis criterion, and also a check of rms distance between the newly generated structure and the structure found so far. The final conformation was obtained through a simulation annealing procedure from 500 to 300 K, and then 3000 rounds of energy minimization were performed to reach a convergence. The final binding modes of the inhibitors were determined on the basis of the energy and the known SAR of the inhibitor. And each binding mode of the inhibitors was evaluated using the score functions[43,44] in the LUDI module within InsightII.

4.4. Multiple copy simultaneous search (MCSS)

The binding site areas in the MCSS simulation were defined as an approximate 32 Å × 16 Å × 12 Å box for Bcl-2, which includes the active site determined in active site analysis and most of the residues around it. 200 copies of a given functional group were randomly distributed inside the binding site and then simultaneously and independently energy-minimized. Pairs of groups were considered to be identical if the rms deviation between

Table 5. Most energetically favorable minima of each cluster for polar functional groups in the positions near the pharmacophoric points

Points	D1	D2	A1	D3	D4	A2	D5
N-Methylacetamide	**38 (−13.1)**	24[a] (−24.5)	**8 (−31.9)**	**3 (−34.1)** 5 (−33.3)			
Methanol	4[b] (−22.3)	**33 (−10.2)**	4[b] (−22.3)	3 (−22.4) 7 (−19.8)	**20 (−16.3)**	47[c] (−7.7)	47[c] (−7.7) **59 (−5.8)**
Dimethyl ether			1 (−17.5)			**43 (−3.4)**	

The serial number and bracketed interaction energy (unit: kcal/mol) of minima are shown. The selected minima are shown in bold.
[a] This group forms two hydrogen bonds with the hydroxyl of Y108 and side chain of R146 simultaneously.
[b] This group forms two hydrogen bonds with the backbone carbonyl of G145 and side chain of R146 simultaneously.
[c] This group forms two hydrogen bonds with the hydroxyl of Y202 simultaneously.

Table 6. Comparison of optimized distances between pharmacophoric points and these of inhibitors **14**–**17**

Distances between pharmacophoric points (Å)	**14**	**15**	**16**	**17**	Improved distances (Å)
H1–H2			4.9	5.1	~**7.7**
H1–H3	8.4	9.5	9.2	10.0	~**9.8**
H2–H3			12.1	14.0	~**13.5**
A1–H1	4.1	4.1	4.2	4.0	~**1.9**
A1–H2			8.6	9.1	~**9.4**
A1–H3	6.8	8.0	8.0	8.4	~**9.3**
D5–H1	9.5	9.6	9.6	9.5	~**9.3**
D5–H2			13.5	14.5	~**14.7**
D5–H3	5.0	6.1	6.1	5.7	~**6.8**
Score 1	445	520	679	581	
Score 2	319	344	432	436	
K_i from Ref. 39 (μM)	24.1 ± 2.1	8.3 ± 1.1	0.93 ± 0.11	0.29 ± 0.06	

The calculated scores and activities of **14**–**17** are listed in the bottom of the table. The scores were computed by the LUDI module of InsightII. The difference between the score 1 and score 2 is that an additional term evaluating the contribution of binding of aromatic-aromatic interaction is added to LUDI score 1.[43,44]

them was less than 0.2 Å, and in such cases, one of the pairs was eliminated. The above protocol was repeated 10 times for each of the functional groups to allow a complete search of the active site. All of the above calculations were performed using the CHARMM22 force field and MCSS 2.1 program.

Acknowledgment

This work was supported in part by the Innovation Fund for Doctorate Candidates of Second Military Medical University of China (for 2005).

References and notes

1. Adams, J. M.; Cory, S. *Science* **1998**, *281*, 1322–1326.
2. Cory, S.; Adams, J. M. *Nat. Rev. Cancer* **2002**, *2*, 647–656.
3. Tsujimoto, Y. *J. Cell Physiol.* **2003**, *195*, 158–167.
4. Petros, A. M.; Nettesheim, D. G.; Wang, Y.; Olejniczak, E. T.; Meadows, R. P.; Mack, J.; Swift, K.; Matayoshi, E. D.; Zhang, H.; Thompson, C. B.; Fesik, S. W. *Protein Sci.* **2000**, *9*, 2528–2534.
5. Petros, A. M.; Olejniczak, E. T.; Fesik, S. W. *Biochim. Biophys. Acta* **2004**, *1644*, 83–94.
6. Sattler, M.; Liang, H.; Nettesheim, D.; Meadows, R. P.; Harlan, J. E.; Eberstadt, M.; Yoon, H. S.; Shuker, S. B.; Chang, B. S.; Minn, A. J.; Thompson, C. B.; Fesik, S. W. *Science* **1997**, *275*, 983–986.
7. Coultas, L.; Strasser, A. *Semin. Cancer Biol.* **2003**, *13*, 115–123.
8. Kirkin, V.; Joos, S.; Zornig, M. *Biochim. Biophys. Acta* **2004**, *1644*, 229–249.
9. Juin, P.; Geneste, O.; Raimbaud, E.; Hickman, J. A. *Biochim. Biophys. Acta* **2004**, *1644*, 251–260.
10. Cory, S.; Huang, D. C.; Adams, J. M. *Oncogene* **2003**, *22*, 8590–8607.
11. Shangary, S.; Johnson, D. E. *Leukemia* **2003**, *17*, 1470–1481.
12. Osford, S. M.; Dallman, C. L.; Johnson, P. W.; Ganesan, A.; Packham, G. *Curr. Med. Chem* **2004**, *11*, 1031–1039.
13. Pellecchia, M.; Reed, J. C. *Curr. Pharm. Des* **2004**, *10*, 1387–1398.
14. Wang, J. L.; Liu, D.; Zhang, Z. J.; Shan, S.; Han, X.; Srinivasula, S. M.; Croce, C. M.; Alnemri, E. S.; Huang, Z. *Proc. Natl. Acad. Sci. U.S.A* **2000**, *97*, 7124–7129.
15. Enyedy, I. J.; Ling, Y.; Nacro, K.; Tomita, Y.; Wu, X.; Cao, Y.; Guo, R.; Li, B.; Zhu, X.; Huang, Y.; Long, Y. Q.; Roller, P. P.; Yang, D.; Wang, S. *J. Med. Chem.* **2001**, *44*, 4313–4324.
16. Tzung, S. P.; Kim, K. M.; Basanez, G.; Giedt, C. D.; Simon, J.; Zimmerberg, J.; Zhang, K. Y.; Hockenbery, D. M. *Nat. Cell Biol.* **2001**, *3*, 183–191.
17. Kim, K. M.; Giedt, C. D.; Basanez, G.; O'Neill, J. W.; Hill, J. J.; Han, Y. H.; Tzung, S. P.; Zimmerberg, J.; Hockenbery, D. M.; Zhang, K. Y. *Biochemistry* **2001**, *40*, 4911–4922.
18. Leone, M.; Zhai, D.; Sareth, S.; Kitada, S.; Reed, J. C.; Pellecchia, M. *Cancer Res.* **2003**, *63*, 8118–8121.
19. Real, P. J.; Cao, Y.; Wang, R.; Nikolovska-Coleska, Z.; Sanz-Ortiz, J.; Wang, S.; Fernandez-Luna, J. L. *Cancer Res.* **2004**, *64*, 7947–7953.
20. Oltersdorf, T.; Elmore, S. W.; Shoemaker, A. R.; Armstrong, R. C.; Augeri, D. J.; Belli, B. A.; Bruncko, M.; Deckwerth, T. L.; Dinges, J.; Hajduk, P. J.; Joseph, M. K.; Kitada, S.; Korsmeyer, S. J.; Kunzer, A. R.; Letai, A.; Li, C.; Mitten, M. J.; Nettesheim, D. G.; Ng, S.; Nimmer, P. M.; O'Connor, J. M.; Oleksijew, A.; Petros, A. M.; Reed, J. C.; Shen, W.; Tahir, S. K.; Thompson, C. B.; Tomaselli, K. J.; Wang, B.; Wendt, M. D.; Zhang, H.; Fesik, S. W.; Rosenberg, S. H. *Nature* **2005**, *435*, 677–681.
21. Nguyen, T. L.; McGrath, C.; Hermone, A. R.; Burnett, J. C.; Zaharevitz, D. W.; Day, B. W.; Wipf, P.; Hamel, E.; Gussio, R. *J. Med. Chem* **2005**, *48*, 6107–6116.
22. Shuker, S. B.; Hajduk, P. J.; Meadows, R. P.; Fesik, S. W. *Science* **1996**, *274*, 1531–1534.
23. Petros, A. M.; Dinges, J.; Augeri, D. J.; Baumeister, S. A.; Betebenner, D. A.; Bures, M. G.; Elmore, S. W.; Hajduk, P. J.; Joseph, M. K.; Landis, S. K.; Nettesheim, D. G.; Rosenberg, S. H.; Shen, W.; Thomas, S.; Wang, X.; Zanze, I.; Zhang, H.; Fesik, S. W. *J. Med. Chem* **2006**, *49*, 656–663.
24. Caflisch, A.; Miranker, A.; Karplus, M. *J. Med. Chem* **1993**, *36*, 2142–2167.
25. Miranker, A.; Karplus, M. *Proteins* **1991**, *11*, 29–34.
26. Joseph-McCarthy, D.; Hogle, J. M.; Karplus, M. *Proteins* **1997**, *29*, 32–58.
27. Zheng, C. H.; Zhou, Y. J.; Zhu, J.; Chen, J.; Li, Y. W.; Sheng, C. Q.; Song, Y. L.; Jiang, Q. F.; Lv, J. G. *Acta Chim. Sinica* **2006**, *64*, 2327–2332.
28. Zheng, C. H.; Zhou, Y. J.; Zhu, J.; Chen, J.; Li, Y. W.; Sheng, C. Q.; Song, Y. L.; Jiang, Q. F.; Lv, J. G. *Acta Chim. Sinica* **2006**, *64*, 2215–2220.
29. Zhai, D.; Jin, C.; Satterthwait, A. C.; Reed, J. C. *Cell Death. Differ.* **2006**, *13*, 1419–1421.
30. Liu, X.; Dai, S.; Zhu, Y.; Marrack, P.; Kappler, J. W. *Immunity* **2003**, *19*, 341–352.
31. Zheng, C. H.; Zhou, Y. J.; Zhu, J.; Chen, J.; Li, Y. W.; Sheng, C. Q.; Song, Y. L.; Jiang, Q. F.; Lv, J. G. *Acad. J. Sec. Mil. Med. Univ.* **2006**, *27*, 1085–1088.
32. Ottilie, S.; Diaz, J. L.; Horne, W.; Chang, J.; Wang, Y.; Wilson, G.; Chang, S.; Weeks, S.; Fritz, L. C.; Oltersdorf, T. *J. Biol. Chem* **1997**, *272*, 30866–30872.
33. Yin, X. M.; Oltvai, Z. N.; Korsmeyer, S. J. *Nature* **1994**, *369*, 321–323.
34. Kelekar, A.; Chang, B. S.; Harlan, J. E.; Fesik, S. W.; Thompson, C. B. *Mol. Cell Biol.* **1997**, *17*, 7040–7046.
35. Manion, M. K.; O'Neill, J. W.; Giedt, C. D.; Kim, K. M.; Zhang, K. Y.; Hockenbery, D. M. *J. Biol. Chem.* **2004**, *279*, 2159–2165.
36. Cheng, E. H.; Levine, B.; Boise, L. H.; Thompson, C. B.; Hardwick, J. M. *Nature* **1996**, *379*, 554–556.
37. Zha, J.; Harada, H.; Osipov, K.; Jockel, J.; Waksman, G.; Korsmeyer, S. J. *J. Biol. Chem.* **1997**, *272*, 24101–24104.
38. Pinto, M.; Perez, J. J.; Rubio-Martinez, J. *J. Comput. Aided Mol. Des.* **2004**, *18*, 13–22.
39. Wang, G.; Nikolovska-Coleska, Z.; Yang, C. Y.; Wang, R.; Tang, G.; Guo, J.; Shangary, S.; Qiu, S.; Gao, W.; Yang, D.; Meagher, J.; Stuckey, J.; Krajewski, K.; Jiang, S.; Roller, P. P.; Abaan, H. O.; Tomita, Y.; Wang, S. *J. Med. Chem.* **2006**, *49*, 6139–6142.
40. *SYBYL*, release version 6.9; Tripos Associates, Inc., St. Louis, Missouri.
41. *InsightII*, release version 2000; Accelrys, Inc., San Diego, California.
42. Luty, B. A.; Wasserman, Z. R.; Stouten, P. F. W.; Hodge, C. N.; Zacharias, M.; McCammon, J. A. *J. Comput. Chem.* **1995**, *16*, 454–464.
43. Böhm, H. J. *J. Comput. Aided Mol. Des.* **1994**, *8*, 243–256.
44. Böhm, H. J. *J. Comput. Aided Mol. Des.* **1998**, *12*, 309–323.
45. Nikolovska-Coleska, Za.; Wang, R.; Fang, X.; Pan, H.; Tomita, Y.; Li, P.; Roller, P. P.; Krajewski, K.; Saito, N.; Stuckey, J.; Wang, S. *Anal. Biochem.* **2004**, *332*, 261–273.